Modulational instabilities in dispersion-flattened fibers

M. Yu and C. J. McKinstrie
Department of Mechanical Engineering, University of Rochester, Rochester, New York 14627
and Laboratory for Laser Energetics, 250 East River Road, Rochester, New York 14623

Govind P. Agrawal
Institute of Optics, University of Rochester, Rochester, New York 14627
(Received 12 August 1994; revised manuscript received 9 February 1995)

The nonlinear Schrödinger equation does not describe fast modulations adequately because it is based on a Taylor expansion in the frequency domain. In this paper, we study the effects of the entire modal dispersion curve and the frequency dependence of the nonlinear coefficients on the formation of modulational instabilities by using harmonic analysis. New regions of instability for dispersion-flattened fibers are found and characterized by this approach. The relation of these instabilities to the conventional modulational and four-wave-mixing instabilities is discussed.

PACS number(s): 42.81.Dp, 52.35.Mw, 42.65.Ky

I. INTRODUCTION

Modulational instability (MI) is a general feature of wave propagation in a dispersive nonlinear medium. It refers to a process in which a weak perturbation of a continuous wave (cw) grows exponentially in the form of amplitude modulation (in the linear regime). This process occurs as a result of the interplay between self-phase modulation and group-velocity dispersion. It is usually modeled by a nonlinear Schrödinger equation (NSE), which is the simplest model that takes into account both mechanisms. The NSE is used in such diverse fields as fluid dynamics, nonlinear optics, and plasma physics [1–3]. In the one-dimensional case, such as that which occurs in an optical fiber, MI is responsible for the breakup of a long pulse into solitons [4]. Optical solitons have potential application in optical communications. MI has also been used in parametric amplification [2], optical switching [5], and short-pulse generation [6].

MI is usually studied within the framework of a NSE, the validity of which requires a weak instantaneous nonlinearity and a slowly varying wave amplitude. In the frequency domain, it amounts to assuming that the spectral width of the field is narrow enough that the modal dispersion relation $\beta(\omega)$ can be approximated by a second-order Taylor expansion around the carrier frequency ω_0. For slightly wider bandwidths, some corrections to the NSE have been made by adding higher-order dispersion terms in the Taylor expansion [7–9].

In some of the cases discussed below, however, MI can actually occur with a wide bandwidth (corresponding to a fast temporal modulation). In other words, the effects of second- and third-order dispersion, etc., could all be comparable in these cases; the Taylor expansion breaks down, and the nonlocal properties of the modal dispersion relation must be considered. For fast modulations, nonlinear relaxation and the Raman effect may also become important [8–11]. Because of the noninstantaneous nonlinearity, the dependence of the nonlinear coefficient on modulational frequency should be included.

Broader-bandwidth MI is important due to its intrinsic relation to shorter pulses. In this paper, we use harmonic analysis instead of the NSE to study MI. This approach still requires weak nonlinearity but does not require a narrow bandwidth. A simple expression for the gain curve of MI is given that depends on the entire modal dispersion curve and the frequency-dependent nonlinear coefficients. It is then applied to a dispersion-flattened fiber [12], for which the second-order dispersion coefficient changes sign twice as the frequency is varied, to study the effects of the modal dispersion relation and to illustrate the basic physics.

II. HARMONIC ANALYSIS

To be precise, the harmonic analysis described below is actually a multiscale approximation [13] to solve the linearized equation around a nonlinear steady-state pump wave in a single mode fiber. The small parameter in the linearized equation is the amplitude of the nonlinear pump wave normalized to $\sqrt{\beta(\omega_0)/\gamma}$ [see Eq. (2)]. In the following summary, however, the physical picture is emphasized at the expense of mathematical details.

It is well known that the nonlinear steady-state or cw pump wave for the single transverse mode of the fiber is approximately a sinusoidal wave with the dispersion relation [2,11]

$$k_s(\omega_0)=\beta(\omega_0)+\gamma(\omega_0,-\omega_0,\omega_0)|A_0|^2 , \tag{1}$$

where the subscript s is for steady state, and the weak nonlinearity condition

$$\gamma|A_0|^2 \ll \beta(\omega_0) \tag{2}$$

is required. Equations (1) and (2) indicate that the $\chi^{(3)}$ nonlinearity changes the wave number (and the phase, which is the product of the wave number and the distance) by a small amount. For an optical fiber,

$\gamma(\omega_0,-\omega_0,\omega_0)=6\pi\omega_0\chi^{(3)}(\omega_0,-\omega_0,\omega_0)/[cn(\omega_0)A_{\text{eff}}]$ in electrostatic units to within a factor of the order of unity that depends on the transverse mode structure, where $\chi^{(3)}(\omega_0,-\omega_0,\omega_0)$ is the third-order nonlinear susceptibility of the fiber, c is the speed of light, $n(\omega_0)$ is the modal refractive index, and A_{eff} is its effective mode area [2].

A linearized equation around the cw solution can then be formed for a perturbation field. The evolution of the perturbation field in the presence of the cw pump described by Eq. (1) can be studied in the Fourier domain by considering the propagation of its frequency components $\delta A(\omega',z)$ for the single transverse mode, where z and ω' represent space and frequency coordinates, respectively. Since the amplitude of the cw field is the small parameter, the trivial case of the zeroth-order approximation, which corresponds to a vanished pump, gives a linear propagation of the perturbation field, i.e., $d_{zz}^2\delta A(\omega',z)+\beta^2(\omega')\delta A(\omega',z)=0$. The zeroth-order solution is thus $\delta A(\omega',z)=\delta A(\omega',0)\exp[i\beta(\omega')z]$, corresponding to forward propagation. Note that the reality condition requires $\delta A(-\omega',z)=\delta A^*(\omega',z)$.

In the presence of the cw pump wave, the linearized equation for $\delta A(\omega',z)$ can be obtained from the Maxwell equation for the single transverse mode,

$$d_{zz}^2\delta A(\omega',z)+\beta^2(\omega')\delta A(\omega',z)=(4\pi/c)\omega'^2\delta P_{\text{nl}}(\omega') , \quad (3)$$

where the term δP_{nl}, still linear in the perturbative field, is the nonlinear part of the electric polarization field projected to the transverse mode by an overlap integration [2].

Recall that $\delta P_{\text{nl}}\simeq 0$ in the zeroth-order approximation. For a better approximation beyond zeroth order, we have

$$\delta P_{\text{nl}}(\omega')=3(1/A^{\text{eff}})\int\int\int_{-\infty}^{+\infty}\chi^{(3)}(\omega_1,\omega_2,\omega_3)E_0(\omega_1,z)E_0(\omega_2,z)\delta A(\omega_3,z)\delta(\omega'-\omega_1-\omega_2-\omega_3)d\omega_1 d\omega_2 d\omega_3 , \quad (4)$$

where we have assumed the overlap integral of the transverse mode is the same for the frequencies of interest [2].

$$E_0(\omega,z)=A_0\exp[ik_s(\omega_0)z]\delta(\omega-\omega_0)+A_0^*\exp[-ik_s(\omega_0)z]\delta(\omega+\omega_0)$$

is the Fourier transform of the cw field $\bar{E}_0(t,z)=A_0\exp[ik_s(\omega_0)z-i\omega_0 t]+\text{c.c.}$ Equation (4) describes the nonlinear electric polarization (but it is linear in a perturbative field) induced by the pump and the perturbative field in the $\chi^{(3)}$ medium. The degeneracy factor 3 appears because we treat the perturbation as a field different from the pump wave [11]. We have neglected higher-order contributions (greater than $|A_0|^2$) of the pump field to δP_{nl}.

To solve Eq. (3) beyond the zeroth-order approximation, we follow the multiscale procedure by inserting the zeroth-order solution in the right-hand side of Eq. (3) [using Eq. (4)] and collecting all the possible phase-matched terms. This analysis can be facilitated by switching to the temporal domain picture. For a forward propagation component at ω', the field is $\delta A(\omega',0)\exp[i\beta(\omega')z-i\omega' t]+\text{c.c.}$ Through the nonlinear electric polarization, this fields generates the terms proportional to

$$\delta A(\omega',z)|A_0|^2\exp[i\beta(\omega')z-i\omega' t]+\text{c.c.} ,$$

$$\delta A^*(\omega',z)A_0^2\exp\{i[2k_s(\omega_0)-\beta(\omega')]z-i(2\omega_0-\omega')t\}+\text{c.c.}$$

The first term is obviously phase matched. The second term could also be phase matched to a forward propagating component at $(2\omega_0-\omega')$ if $|2k_s(\omega_0)-\beta(\omega')-\beta(2\omega_0-\omega')|$ is very small. Thus we should study the component

$$\delta A(2\omega_0-\omega',z)=\delta A(2\omega_0-\omega',0)\exp[i\beta(2\omega_0-\omega')z-i(2\omega_0-\omega')t]+\text{c.c.}$$

Similar analysis for this component indicates two phase-matched terms generated at $(2\omega_0-\omega')$ and ω'.

According to the multiscale procedure, the above consideration allows one to solve Eq. (3) approximately by the coupled mode equation of the frequency components at ω' and $2\omega_0-\omega'$, called anti-Stokes and Stokes sidebands, respectively. By retaining all the possible phase-matched driving terms, Eqs. (3) and (4) become

$$[d_{zz}^2+\beta^2(\omega')]\delta A(\omega',z)/[2\beta(\omega')]=2\gamma(\omega_0,-\omega_0,\omega')|A_0|^2\delta A(\omega',z)+\gamma[\omega_0,\omega_0,-(2\omega_0-\omega')]A_0^2\times\exp[i2k_s(\omega_0)]\delta A^*(2\omega_0-\omega',z) , \quad (5)$$

$$[d_{zz}^2+\beta^2(2\omega_0-\omega')]\delta A(2\omega_0-\omega',z)/[2\beta(2\omega_0-\omega')]=2\gamma(\omega_0,-\omega_0,2\omega_0-\omega')|A_0|^2\delta A(2\omega_0-\omega',z)+\gamma(\omega_0,\omega_0,-\omega')A_0^2\exp[i2k_s(\omega_0)]\delta A^*(\omega',z) , \quad (6)$$

where we have defined

$$\gamma(\omega_1,\omega_2,\omega_3)=6\pi(\omega_1+\omega_2+\omega_3)\times\chi^{(3)}(\omega_1,\omega_2,\omega_3)/[cn(\omega_1+\omega_2+\omega_3)A_{\text{eff}}] . \quad (7)$$

Equations (5) and (6) will give a correction to the linear dispersion relation $\beta(\omega')$ [or $\beta(2\omega_0-\omega')$ for frequency $2\omega_0-\omega'$] by the amount $O(\gamma|A_0|^2)$. Simplification can be made for the forward propagation by using

$$(d_{zz}^2+\beta^2)/(2\beta)=(-id_z+\beta)(id_z+\beta)/(2\beta)\simeq id_z+\beta ,$$

where β indicates $\beta(\omega')$ or $\beta(2\omega_0-\omega')$ since a careful

analysis shows this would not affect the accuracy in the present order of approximation. If we define the modulational frequency $\omega \equiv \omega' - \omega_0$, and set $\delta A(\omega',z) \equiv B_+(\omega,z)\exp(ik_s z)$ and $\delta A(2\omega_0-\omega',z) \equiv B_-(\omega,z)\exp(ik_s z)$, then Eqs. (5) and (6) become

$$D_+(-id_z,\omega)B_+ = \gamma_{f+}A_0^2 B_-^* , \tag{8}$$

$$D_-(-id_z,\omega)B_-^* = -\gamma_{f-}^* A_0^{*2} B_+ , \tag{9}$$

where

$$D_+(-id_z,\omega) \equiv -id_z + \beta(\omega_0) - \beta(\omega_0+\omega) - \gamma_{x+}|A_0|^2 , \tag{10}$$

$$D_-(-id_z,\omega) \equiv -id_z - \beta(\omega_0) + \beta(\omega_0-\omega) + \gamma_{x-}^*|A_0|^2 \tag{11}$$

and

$$\gamma_{x+} \equiv 2\gamma[\omega_0,-\omega_0,(\omega_0+\omega)] - \gamma(\omega_0,-\omega_0,-\omega_0) , \tag{12}$$

$$\gamma_{x-} \equiv 2\gamma[\omega_0,-\omega_0,(\omega_0-\omega)] - \gamma(\omega_0,-\omega_0,\omega_0) , \tag{13}$$

$$\gamma_{f+} \equiv \gamma[\omega_0,\omega_0,-(\omega_0-\omega)] , \tag{14}$$

$$\gamma_{f-} \equiv \gamma[\omega_0,\omega_0,-(\omega_0+\omega)] . \tag{15}$$

The subscripts x and f refer to cross-phase modulation (XPM) and four-wave mixing (FWM) to indicate their relation to these processes, respectively. Note that the Raman effect and the effect of nonlinear relaxation are included through the dependence of the nonlinear coefficients on the modulational frequency.

Equations (8) and (9) can be easily solved. The general solution consists of two independent eigenmodes,

$$\begin{bmatrix} B_+ \\ B_-^* \end{bmatrix} = c_1 \begin{bmatrix} 1 \\ r_+(\omega) \end{bmatrix} e^{ik_+(\omega)z} + c_2 \begin{bmatrix} r_-(\omega) \\ 1 \end{bmatrix} e^{ik_-(\omega)z} , \tag{16}$$

where c_1 and c_2 are constants, and

$$r_+ = D_+(k_+,\omega)/\gamma_{f+}A_0^2 = -\gamma_{f-}^* A_0^{*2}/D_-(k_+,\omega) , \tag{17}$$

$$r_- = \gamma_{f+}A_0^2/D_+(k_-,\omega) = -D_-(k_-,\omega)/\gamma_{f-}^* A_0^{*2} \tag{18}$$

indicate the relative amplitudes of Stokes and anti-Stokes sidebands for each eigenmode, respectively. $k_\pm(\omega)$ are the dispersion relations for the two eigenmodes,

$$k_\pm(\omega) = [\beta(\omega_0+\omega) - \beta(\omega_0-\omega) + (\gamma_{x+} - \gamma_{x-}^*)|A_0|^2 \pm \sqrt{\Delta^2 - 4\gamma_{f+}\gamma_{f-}^*|A_0|^4}]/2 , \tag{19}$$

where

$$\Delta(\omega) \equiv \Delta_l - \gamma_{x+}|A_0|^2 - \gamma_{x-}^*|A_0|^2 , \tag{20}$$

is the total wave-number mismatch and

$$\Delta_l(\omega) \equiv 2\beta(\omega_0) - \beta(\omega_0+\omega) - \beta(\omega_0-\omega) \tag{21}$$

is the linear wave-number mismatch (the subscript l is for linear). Naturally, a negative imaginary part of $k_\pm(\omega)$ indicates the growth of the corresponding eigenmode.

Physically, the coupled Eqs. (8) and (9) describe the linearized stage of the induced decay of the carrier wave at the frequency ω_0 into its daughter waves at the sideband frequencies $\omega_0 \pm \omega$. The right-hand side of each equation presents the harmonic driving from the nonlinear beating or FWM of the carrier and the other daughter wave, and the left-hand side describes propagation with total wave-number mismatch (including linear and nonlinear mismatch). The nonlinear wave-number mismatch comes from XPM, and is generally complex due to the Raman effect or nonlinear relaxation. Alternatively, Eqs. (8) and (9) describe the scattering of the pump into one of the sidebands by the nonlinear grating produced by the pump and the other sideband. These equations decouple automatically when $|\gamma|A_0|^2/\Delta_l| \ll 1$. In this limit, without loss of accuracy, the two independent eigenmode of Eqs. (8) and (9) become

$$k_+ = -\beta(\omega_0) + \beta(\omega_0+\omega) + \gamma_{x+}|A_0|^2 , \quad r_+ \simeq 0 \text{ or } B_- \simeq 0 \tag{22}$$

and

$$k_- = \beta(\omega_0) - \beta(\omega_0-\omega) - \gamma_{x-}^*|A_0|^2 , \quad r_- \simeq 0 \text{ or } B_+ \simeq 0 . \tag{23}$$

Physically, these solutions correspond to the independent evolution of each sideband subject to the Raman loss (for the anti-Stokes) or gain (for the Stokes) and with the refractive index changed by the pump due to XPM.

Generally, each frequency component cannot propagate independently, but couples to the other sideband. In fact, expressing c_1 and c_2 in terms of the input condition leads to the general solution in the form of a transfer matrix,

$$\begin{bmatrix} B_+(\omega,z) \\ B_-^*(\omega,z) \end{bmatrix} = \frac{1}{1-r_+r_-} \begin{bmatrix} e^{ik_+z} - r_+r_-e^{ik_-z} & r_-(e^{ik_-z} - e^{ik_+z}) \\ r_+(e^{ik_+z} - e^{ik_-z}) & e^{ik_-z} - r_+r_-e^{ik_+z} \end{bmatrix} \begin{bmatrix} B_+(\omega,0) \\ B_-^*(\omega,0) \end{bmatrix} . \tag{24}$$

This equation linearly relates the Fourier spectrum at any distance z to the input spectrum.

In the case of instability and at large distances, the contribution from the damped eigenmode can be neglected. Then $\mathrm{Im}[k_+(\omega)]$ gives the information about the spectrum amplification with distance, while $|r_+(\omega)|$ indicates the relative amplitude of Stokes and anti-Stokes sidebands, if the + sign is used to represent the growing

mode.

To isolate the effect of the shape of the modal dispersion curve $\beta(\omega')$, we first neglect the frequency dependence of the nonlinear coefficients by using their value at zero modulational frequency $\omega=0$. It is easy to show that $\gamma_{x\pm}=\gamma_{f\pm}=\gamma(\omega_0,-\omega_0,\omega_0)$, which is a real parameter denoted by γ. This means that the Raman effect and other dependence of nonlinear coefficients on frequency are neglected. Then Eq. (19) becomes

$$k_{\pm}=[\beta(\omega_0+\omega)-\beta(\omega_0-\omega) \pm\sqrt{(\Delta_l-2\gamma|A_0|^2)^2-(2\gamma|A_0|^2)^2}]/2 , \quad (25)$$

where the term $\Delta_l-2\gamma|A_0|^2$ under the square root is just the total wave-number mismatch Δ, which is real in this case. Instability happens whenever its amplitude is smaller than that of the FWM coupling strength $2\gamma|A_0|^2$. (This condition means that the linear mismatch compensates for the nonlinear mismatch.) It can be proved that $|r_+(\omega)|=1$ for ω in the unstable range, so the amplitudes of the Stokes and anti-Stokes waves are equal for the growing mode. In the following, we only consider the $\gamma>0$ case. Since the $\gamma<0$ case is similar, our discussion can be easily extended.

The instability happens when

$$0<\Delta_l(\omega)<4\gamma|A_0|^2 . \quad (26)$$

In a digram of $\Delta_l(\omega)$ (see, for example, Fig. 1), the instability range is between the horizontal axis and the horizontal line at $4\gamma|A_0|^2$. If in this range $\Delta_l(\omega)$ reaches the value $2\gamma|A_0|^2$, then the maximum growth rate

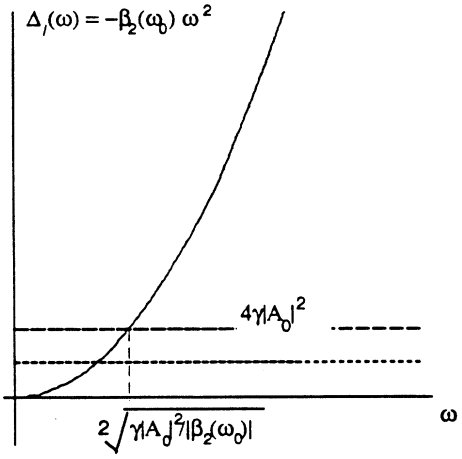

FIG. 1. Instability analysis using $\Delta_l(\omega)=-\beta_2(\omega_0)\omega^2$. The upper dashed horizontal line is $4\gamma|A_0|^2$ and the lower is $2\gamma|A_0|^2$. The frequency range of instability corresponds to the section of the $\Delta_l(\omega)$ curve between the horizontal axis and upper dashed horizontal line. The intersections of the curve with the lower dashed horizontal line indicate the frequency of maximum growth rate $\gamma|A_0|^2$. As power increases, both horizontal lines go up.

$[\mathrm{Im}(k)]_{\max}=\gamma|A_0|^2$ is obtained, corresponding to a complete linear compensation of the nonlinear wave-number mismatch; if it does not (as can happen in the dispersion-flattened fiber), the maximum growth rate happens at Δ_{le} (the subscript e is for extremum), which is the extremum of $\Delta_l(\omega)$ closest to the horizontal line at $2\gamma|A_0|^2$, with a value

$$[\mathrm{Im}(k)]_{\max}=\sqrt{(2\gamma|A_0|^2-\Delta_{le})^2-(2\gamma|A_0|^2)^2}/2 < \gamma|A_0|^2 . \quad (27)$$

This corresponds to a maximal, but incomplete, compensation.

In many situations, the second-order dispersion function, defined as $\beta_2(\omega')\equiv(d/d\omega')^2\beta(\omega')$, is given instead of the modal dispersion $\beta(\omega')$. Thus we wish to express $\Delta_l(\omega)$ in terms of the second-order dispersion function. Since $(d/d\omega)^2\Delta_l(\omega)=-\beta_2(\omega_0+\omega)-\beta_2(\omega_0-\omega)$ and $(d/d\omega)\Delta_l(0)=\Delta_l(0)=0$ from Eq. (21), one can show that

$$\Delta_l(\omega)=\int_0^{\omega}[\beta_2(\omega_0+\nu)+\beta_2(\omega_0-\nu)](\nu-\omega)d\nu . \quad (28)$$

For very small modulation frequency, a parabolic approximation for the modal dispersion curve $\beta(\omega')$ can be used around the pump frequency. This is equivalent to considering $\beta_2(\omega')$ a constant within the frequency range of investigation: $\beta_2(\omega_0\pm\omega)=\beta_2(\omega_0)$. It follows from Eq. (28), $\Delta_l(\omega)=-\beta_2(\omega_0)\omega^2$, which is displayed in Fig. 1 for the case of $\beta_2(\omega_0)<0$. This figure also indicates that the instability range is at $2\sqrt{\gamma|A_0|^2/|\beta_2(\omega_0)|}$ and the maximum growth is $\gamma|A_0|^2$. These results agree with those obtained from the standard NSE model [2].

However, as the power increases [but Eq. (2) must be satisfied] or the second-order dispersion coefficient at the pump frequency decreases, the instability range becomes wider, and finally the approximation that $\beta(\omega')$ is parabolic, or $\beta_2(\omega')$ is constant, breaks down. In addition, this treatment will miss any MI gain occurring at relatively large ω. So, to explore the broad-bandwidth behavior of the MI gain, the exact linear dispersion relation should be used [14]. A good example is the dispersion-flattened fiber discussed in the following section.

III. DISPERSION-FLATTENED FIBER

A. $\beta_{2e}<0$ case

A dispersion-flattened fiber [12] has the characteristic second-order dispersion function shown in Fig. 2. Notice that $\beta_2(\omega)$ cannot be considered constant in the frequency range of interest because it changes sign twice. As a simple model, we fit the curve with a parabola. With this assumption,

$$\beta_2(\omega')=\beta_{2e}[1-(\omega'-\omega_p')^2/\omega_z^2] , \quad (29)$$

where β_{2e} is the minimal value of $\beta_2(\omega')$ occurring at the frequency ω_p', and $2\omega_z$ is the frequency spacing between the two points of zero dispersion (the subscripts e and z are for extremum and zero, respectively). In an ordinary

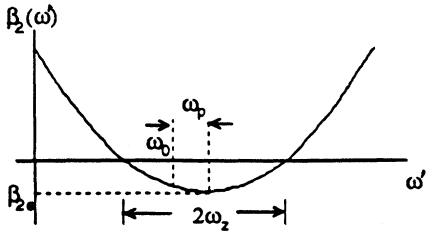

FIG. 2. Illustration of $\beta_2(\omega')$ for dispersion-flattened fiber. β_{2e} and ω_p are the extreme β_2 value and the corresponding frequency relative to the pump frequency, respectively. $2\omega_z$ is the difference between the two zero-dispersion frequencies.

dispersion-flattened fiber β_{2e} is negative.

Using Eqs. (28) and (29), we get

$$\Delta_l(\omega)=-\beta_{2e}(1-\omega_p^2/\omega_z^2)\omega^2\left[1-\frac{\omega^2}{6\omega_z^2(1-\omega_p^2/\omega_z^2)}\right], \tag{30}$$

where $\omega_p=\omega_p'-\omega_0$ is the minimum dispersion frequency relative to the pump frequency. An instability analyses based on $\Delta_l(\omega)$is displayed in Fig. 3. Its two zero points are at $\omega=0$ and ω_f (the subscript f is for FWM), where

$$\omega_f^2=6\omega_z^2(1-\omega_p^2/\omega_z^2)\ . \tag{31}$$

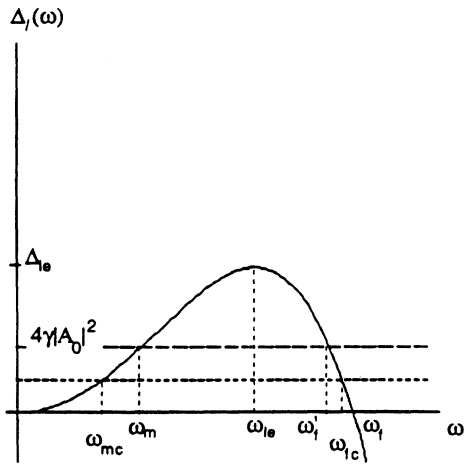

FIG. 3. Instability analysis using $\Delta_l(\omega)$ in the case of a dispersion-flattened fiber. The upper and lower dashed horizontal lines are $4\gamma|A_0|^2$ and $2\gamma|A_0|^2$, respectively. The two frequency ranges of instability correspond to the two sections of the $\Delta_l(\omega)$ curve between the horizontal axis and upper dashed horizontal line, i.e., $(0,\omega_m)$ and (ω_f',ω_f). The two intersections of the curve with the lower dashed horizontal line at ω_{mc} and ω_{fc} indicate the frequencies of maximum growth rate $\gamma|A_0|^2$. As power increases, both horizontal lines go up and the two instability regions merge. With further power increase, the intersections of the curve with the lower dashed horizontal line also disappear.

Usually the zeros of linear mismatch at nonzero ω's imply the presence of FWM instabilities for some parameter values. The maximum of Δ_l happens at ω_{le} (the subscript l is for linear and e is for extremum), where

$$\omega_{le}^2=3\omega_z^2(1-\omega_p^2/\omega_z^2)=\omega_f^2/2\ , \tag{32}$$

with the maximum value of

$$\Delta_{le}=-3\omega_z^2(1-\omega_p^2/\omega_z^2)^2\beta_{2e}/2\ . \tag{33}$$

For the relatively low pump power $4\gamma|A_0|^2<\Delta_{le}$, there are two intersection points with the horizontal line of $4\gamma|A_0|^2$ at ω_m (the subscript m is for MI) and ω_f', where

$$\omega_m^2=\omega_{le}^2(1-\sqrt{1-4\gamma|A_0|^2/\Delta_{le}})\ , \tag{34}$$

$$\omega_f'^2=\omega_{le}^2(1+\sqrt{1-4\gamma|A_0|^2/\Delta_{le}|})\ . \tag{35}$$

This indicates two regions of instability with the boundaries $(0,\omega_m)$ and (ω_f',ω_f). The maximum growth rates in both ranges are $\gamma|A_0|^2$ at ω_{mc} and ω_{fc}, respectively, where

$$\omega_{mc}^2=\omega_{le}^2(1-\sqrt{1-2\gamma|A_0|^2/\Delta_{le}})\ , \tag{36}$$

$$\omega_{fc}^2=\omega_{le}^2(1+\sqrt{1-2\gamma|A_0|^2/\Delta_{le}})\ . \tag{37}$$

If the pump power continues to decrease, a comparison of Fig. 3 with Fig. 1 indicates that the first region reduces to the conventional MI discussed in Sec. II. In fact, one can prove that the instability range approaches the conventional form of $\omega_m\sim 2\sqrt{\gamma|A_0|^2/|\beta_2(\omega_0)|}$, where $\beta_2(\omega_0)$ is actually the second-order dispersion coefficient at the pump frequency from Eq. (29) (see Fig. 2). The growth rate is approximated also by the conventional expression. This is expected, since the linear phase-mismatch Δ_l is approximated by the conventional form of $-\beta_2(\omega_0)\omega^2$ within this instability range [this can be deduced from the Taylor expansion $\Delta_l(\omega)\simeq\Delta_l''(0)\omega^2/2$, where $\Delta_l''(0)=-2\beta_2(\omega_0)$ from the definition of Δ_l and β_2].

The second region can be shown to reduce to the conventional FWM instability. In the weak pump power,

$$\omega_f-\omega_f'\sim\omega_{le}\gamma|A_0|^2/\sqrt{2}\Delta_{le}$$

and

$$\Delta_l(\omega)\sim(-4\sqrt{2}\Delta_{le}/\omega_{le})(\omega-\omega_f)$$

in the range (ω_f',ω_f). Recall that for a conventional FWM of a pump wave at ω_0 and the two daughter waves at about $\omega_0\pm\omega_f$, the linear wave-number mismatch and instability bandwidth is $\Delta v_g^{-1}(\omega-\omega_f)$ and $4\gamma|A_0|^2/|\Delta v_g^{-1}|$, respectively, where $\Delta v_g^{-1}\equiv\beta'(\omega_0-\omega_f)-\beta'(\omega_0+\omega_f)$ is the difference of the inverse group velocities between the two daughter waves (the prime means derivative). We have obtained exactly these forms considering $\Delta v_g^{-1}=\Delta'(\omega_f)=-4\sqrt{2}\Delta_{le}/\omega_{le}$. The growth rate also takes the conventional form. We know that in the presence of conventional MI, a long optical pulse will break up to form solitons, but in our case, a competing process of the conventional FWM will channel the energy

into the sidebands at approximately ω_f. These sidebands will beat to form high-repetition-rate short pulses; however, this is a reversible process at the nonlinear stage [15] because after the pump depletion, the sideband's energy will be transferred back to the pump.

If we increase the pump power, the two regions begin to merge as ω_m and ω_f' come closer until they coincide at ω_{le} for the power corresponding to $4\gamma|A_0|^2=\Delta_{le}$ (ω_f does not change with power). After that, the instability range will be locked at $(0,\omega_f)$, independent of power increase. The two peaks of the gain curve with a value of $\gamma|A_0|^2$ are still seperated, since ω_{mc} and ω_{fc} are different, but if the power continues to increase, they also coincide at ω_{le} when $2\gamma|A_0|^2=\Delta_{le}$. After that, the $\Delta_l(\omega)$ curve has no intersection with the horizontal line at $2\gamma|A_0|^2$; thus, the maximum growth rate is smaller than $\gamma|A_0|^2$ and is given by Eq. (27). At even higher powers it is approximately $\sqrt{\gamma|A_0|^2\Delta_{le}}$. The peak is locked at ω_{le}, independent of power increase.

With the analytical expressions of $\omega_{mc},\omega_m,\omega_f',\omega_{fc},\omega_f$, the above analysis is graphically displayed in Fig. 4, indicating the instability region and the ridge of peak growth in a contour plot of the growth rate versus frequency and power. To reduce the number of free parameters, normalized units have been introduced. We normalized ω as $\Omega=\omega/(\omega_z\sqrt{1-\omega_p^2/\omega_z^2})$, β_{2e} as $\beta_{2en}=\beta_{2e}\omega_z^2(1-\omega_p^2/\omega_z^2)^2$, $\gamma|A_0|^2$ as $P=\gamma|A_0|^2/|\beta_{2en}|$, and the growth rate as $G=\mathrm{Im}(k)/|\beta_{2en}|$. Thus, in the normalized units, all the formulas can be rewritten with the formal substitution of $\omega_p=0$, $\beta_{2e}=\mathrm{sgn}(\beta_{2e})=-1$, $\omega_z=1$, $\gamma|A_0|^2=P$, and $\omega=\Omega$. For example, Eq. (30) becomes

$$\Delta_l(\Omega)=-\mathrm{sgn}(\beta_{2e})(1-\Omega^2/6)\Omega^2 . \tag{38}$$

From Eq. (25),

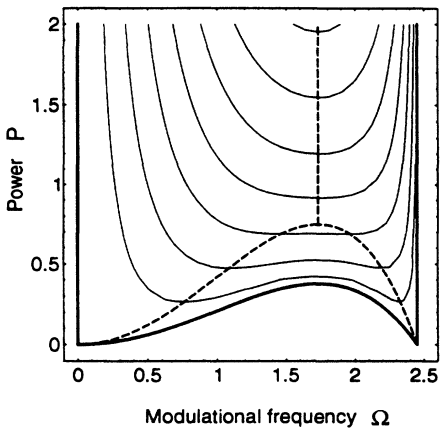

FIG. 4. Instability region in Ω-P space for a dispersion-flattened fiber. The thick lines and the vertical axis enclose the instability region. Within the region, the dashed lines are the position of the peak-growth frequency for varying power. The background curves are the contour plots of the growth rate from Eq. (39).

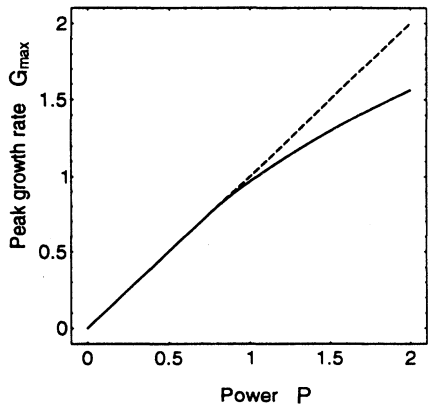

FIG. 5. Peak growth rate $G_{\max}$ versus power P. The point where the deviation from the straight line occurs corresponds to the bifurcation point on the dashed line in Fig. 4. $G_{\max}$ increases with P more slowly after this point because there is not enough linear wave-number mismatch to compensate the nonlinear part.

$$G=\mathrm{Im}\sqrt{[\Delta_l(\Omega)-2P]^2-(2P)^2}/2 . \tag{39}$$

Equations (31)–(37) become

$$\Omega_f^2=6 , \quad \Omega_{le}^2=3 , \quad \Delta_{le}=-\mathrm{sgn}(\beta_{2e})3/2 ,$$
$$\Omega_m^2=3[1-\sqrt{1+\mathrm{sgn}(\beta_{2e})8P/3}] ,$$
$$\Omega_f'^2=3[1+\sqrt{1+\mathrm{sgn}(\beta_{2e})8P/3}] ,$$
$$\Omega_{mc}^2=3[1-\sqrt{1+\mathrm{sgn}(\beta_{2e})4P/3}] ,$$
$$\Omega_{fc}^2=3[1+\sqrt{1+\mathrm{sgn}(\beta_{2e})4P/3}] ,$$

respectively. Notice that Ω and P are now the only free parameters to change. The peak growth rate versus power is displayed in Fig. 5 by using $G_{\max}=P$ and $G_{\max}=\sqrt{-(\frac{3}{2}-2P)^2+(2P)^2}/2$ [from Eq. (27)] for the

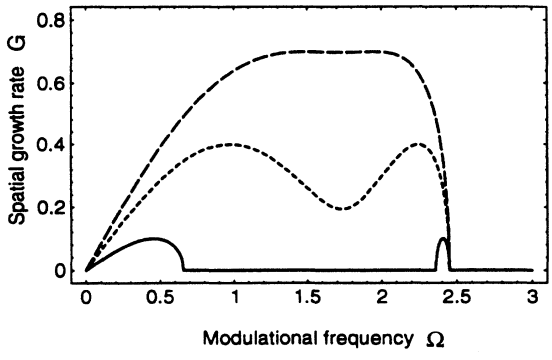

FIG. 6. Growth rate G versus frequency Ω for different powers. The long dashed line, short dashed line, and solid line correspond to $P=0.7$, 0.4, and 0.1, respectively. For low power, it is a superposition of conventional MI (left portion of the solid line) and conventional FWM instability (right portion of the solid line).

ranges of $P \leq \frac{3}{4}$ and $P > \frac{3}{4}$, respectively. Notice that the peak growth rate increases more slowly for higher power because of the incomplete compensation of linear and nonlinear phase mismatches. Figure 6 displays the gain curves at different powers from Eqs. (38) and (39).

B. $\beta_{2e} > 0$ case

While it is true that most dispersion-flattened fibers have $\beta_{2e} < 0$, it is interesting to consider the case in which β_{2e} is a positive number, since our analysis can be used to analyze dispersion curves with any shape. This situation corresponds to a pump propagating in the normal dispersion region bounded by anomalous dispersion regions in frequency space. Following the procedure developed above, we display the instability analysis based on $\Delta_l(\omega)$ in Fig. 7.

Its two zero points are at $\omega=0$ and ω_f given by Eq. (31). Again, the zero of linear mismatch at nonzero ω indicates the possible presence of FWM instability. This is true as shown in Fig. 7, since ω_f', the intersection point with the horizontal line of $4\gamma|A_0|^2$, always exists and is also given by Eqs. (33) and (35) for $\beta_{2e} > 0$.

Unlike in the previous case, the instability corresponding to the ordinary MI does not exist due to the normal dispersion at the pump frequency. The existing instability reduces to the conventional FWM instability at small input power. As the power increases, the peak growth rate is always $\gamma|A_0|^2$ because of complete linear and nonlinear wave-number compensation. The instability region, between ω_f and ω_f' given by Eqs. (31) and (35), keeps increasing with increasing power. The instability region based on these equations and growth rate versus frequency by Eq. (25) are shown in Figs. 8 and 9.

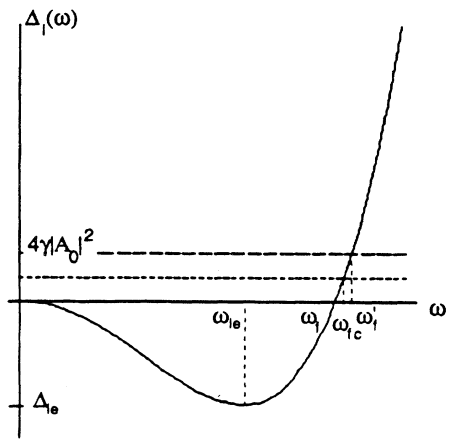

FIG. 7. Instability analysis using $\Delta_l(\omega)$ for $\beta_{2e} > 0$. The upper and lower dashed horizontal lines are $4\gamma|A_0|^2$ and $2\gamma|A_0|^2$, respectively. The frequency range of instability corresponds to the section of $\Delta_l(\omega)$ curve between horizontal axis and upper dashed horizontal line, i.e., (ω_f, ω_f'). The intersection of the curve with the lower dashed horizontal line at ω_{fc} indicates the frequency of maximum growth rate $\gamma|A_0|^2$. As power increases, both horizontal lines go up.

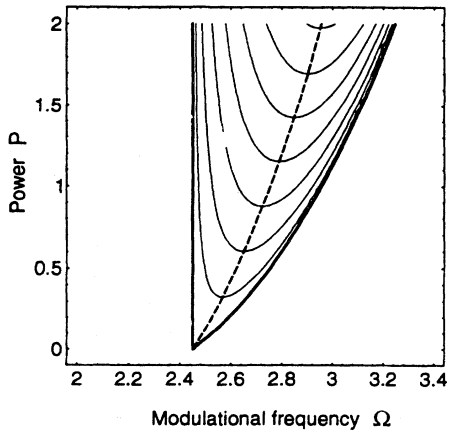

FIG. 8. Same as Fig. 4, except for the sign of β_{2e}. The thick lines enclose the instability region. Within the region, the dashed line is the position of the peak-growth frequency for varying power. The peak growth rate is always P. The background curves are the contour plots of the growth rate from Eq. (39).

Although we have found instability with the pump in the normal dispersion region, it can be proved that at least one of the unstable sidebands is located in the anomalous dispersion region on the $\beta_2(\omega')$ curve.

In summary, the instability behavior at the weak power limit is determined by the analytical properties of $\Delta_l(\omega)$ near the frequencies for which it equals zero. If its first derivative is a nonzero value at such a frequency, which leads to a finite group-velocity difference between the linearly phase-matched sidebands, then we have conventional FWM instability close to that frequency. If the first derivative is also zero, which means equal group velocity of the linear phase-matched sidebands, then we have stability or conventional MI (close to that frequency) depending on whether its second derivative is negative or positive.

We now briefly consider a fiber with many alternating dispersion regions (in frequency space). Based upon the

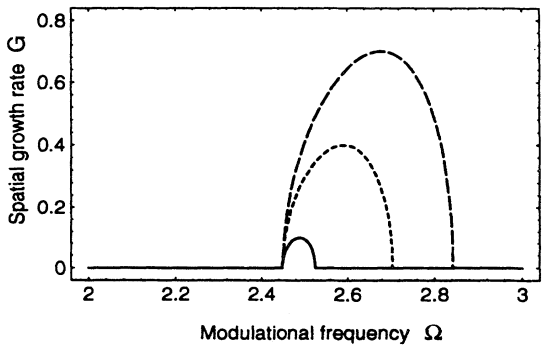

FIG. 9. Same as Fig. 6, except for the sign of β_{2e}. For low power, it is a conventional FWM instability.

above analysis, it is easy to predict instabilities for such a fiber: usually, more instability regions corresponding to FWM will be added to the above pictures because of the oscillating behavior of $\Delta_l(\omega)$. These regions can merge at high pump power. Thus the scheme can produce continuum generation with a wide bandwidth.

C. Frequency-dependent nonlinearity

In the above analysis we neglected the dependence of γ on the modulational frequency and took it as a real quantity. At large ω, the Raman effects come into play and this assumption is invalid. In order to describe the dependence of the nonlinear coefficients on the modulational frequency, a standard model is to assume the nonlinearity comes from an instantaneous electronic response that does not depend on the modulational frequency, plus a retarded nonlinearity that can be described by the simple Lorentzian model for the Raman effect. Thus we can write

$$\chi^{(3)}(\omega_1,\omega_2,\omega_3)=\chi_I^{(3)}+\chi_R^{(3)}(\omega_1,\omega_2,\omega_3) . \tag{40}$$

According to the Lorentzian model [11], the Raman part takes the familiar forms

$$\chi_R^{(3)}[\omega_0,-\omega_0,(\omega_0\pm\omega)] =\tfrac{1}{2}[\chi_{R0}^{(3)}/(1-\omega^2/\omega_R^2\mp i2\nu_R\omega/\omega_R^2)+\chi_{R0}^{(3)}] , \tag{41}$$

$$\chi_R^{(3)}[\omega_0,\omega_0,-(\omega_0\pm\omega)] =\chi_{R0}^{(3)}/(1-\omega^2/\omega_R^2\pm i2\nu_R\omega/\omega_R^2) , \tag{42}$$

$$\chi_R^{(3)}[\omega_0,-\omega_0,\omega_0]=\chi_{R0}^{(3)} , \tag{43}$$

where ω_R and ν_R are the Raman peak frequency and dissipation rate, respectively. $\chi_I^{(3)}$ and $\chi_{R0}^{(3)}$ are parameters for the magnitude of instantaneous and retarded nonlinearity, respectively. Note that $\chi^{(3)}(\omega_0,-\omega_0,\omega_0)=\chi_I^{(3)}+\chi_{R0}^{(3)}$.

From Eq. (7), we have

$$\gamma[\omega_0,-\omega_0,(\omega_0\pm\omega)] \simeq 6\pi\omega_0\chi^{(3)}[\omega_0,-\omega_0,(\omega_0\pm\omega)]/[cn(\omega_0)A_{\rm eff}] , \tag{44}$$

$$\gamma[\omega_0,\omega_0,-(\omega_0\pm\omega)] \simeq 6\pi\omega_0\chi^{(3)}[\omega_0,\omega_0,-(\omega_0\pm\omega)]/[cn(\omega_0)A_{\rm eff}] , \tag{45}$$

where we have kept the ω dependence only in $\chi^{(3)}$ since $(\omega_0\pm\omega)/n(\omega_0\pm\omega)\simeq\omega_0/n(\omega_0)$ in the range of the modulational frequency under consideration.

When combined with Eqs. (44) and (45), Eqs. (40)–(43) allow us to find $\gamma_{x\pm}$ and $\gamma_{f\pm}$ from their definitions in Eqs. (12)–(15),

$$\gamma_{x\pm}=\gamma_{f\pm}=\gamma_I+\gamma_{R0}/(1-\omega^2/\omega_R^2\mp i2\nu_R\omega/\omega_R^2) , \tag{46}$$

where $\gamma_{R0}=6\pi\omega_0\chi_{R0}^{(3)}/[cn(\omega_0)A_{\rm eff}]$ and $\gamma_I=6\pi\omega_0\chi_I^{(3)}/[cn(\omega_0)A_{\rm eff}]$. Note that the nonlinear coefficient for zero modulational frequency is $\gamma(\omega_0,-\omega_0,\omega_0)=\gamma_I+\gamma_{R0}$, which is a real number and will be denoted by γ. By using Eq. (19), the dispersion relation, including the Raman effect, is thus

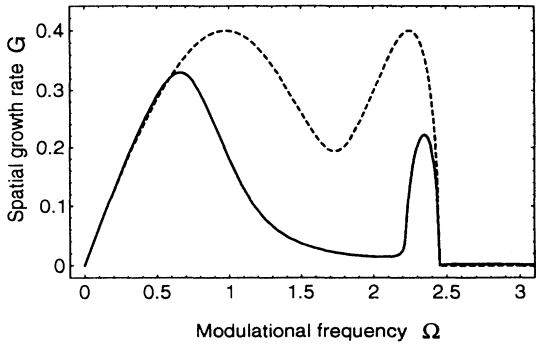

FIG. 10. Growth rate G versus frequency Ω for a fixed power $P=0.4$. The Raman parameters are $\gamma_{R0}=0.4\gamma$, $\gamma_I=0.6\gamma$, and $\nu_R=0.38\omega_R$. The normalized Raman frequency is $\omega_R/(\omega_z\sqrt{1-\omega_p^2/\omega_z^2})=0.78$. The dashed line corresponds to the instantaneous nonlinearity.

$$k_\pm=\tfrac{1}{2}[\beta(\omega_0+\omega)-\beta(\omega_0-\omega) \pm\sqrt{(\Delta_l-2\gamma_{x+}|A_0|^2)^2-(2\gamma_{x+}|A_0|^2)^2}] , \tag{47}$$

where γ_{x+} is given by Eq. (46). It is easy to show that for a very small modulational frequency, $\gamma_{x+}\simeq\gamma$, thus the result for instantaneous nonlinearity is recovered.

As a numerical example, let us suppose that the two points of zero dispersion of the dispersion-flattened fibers are 150 nm apart and the pump frequency is 50 nm off from the extreme-dispersion frequency. This corresponds to $\omega_z/(2\pi)\sim22.5$ THz and $\omega_p/(2\pi)\sim15$ THz. The FWM frequency will be $\omega_f/(2\pi)\sim41$ THz, according to Eq. (31). Assuming that the extremum of the second-order dispersion $\beta_{2e}\sim-1$ ps^2/km, and $\gamma\sim10$ W^{-1}km^{-1}, then the power for the merging of conventional MI and FWM is $|A_0|^2=\Delta_{le}/(4\gamma)\sim231$ W. This power is greatly reduced if the dispersion-flattened range is narrower or the magnitude of the second-order dispersion is smaller.

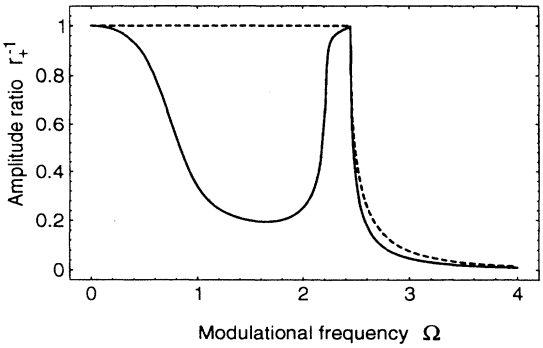

FIG. 11. The amplitudes ratio $|r_+|^{-1}$ of the anti-Stokes and the Stokes wave for the growing mode. The parameters are the same as those of Fig. 7. The dashed line indicates that in the absence of the Raman effect, the ratio is unity in the instability region.

The Raman frequency is about $\omega_R \sim 2\pi \times 13$ THz. And as representative values, $\nu_R \sim 2\pi \times 5$ THz, $\gamma_I \sim 0.6\gamma$, and $\gamma_{R0} \sim 0.4\gamma$. Figure 10 shows the Raman effect on the gain curve obtained from Eq. (47) for the above parameters. By the normalization scheme used before, the frequency Ω, the growth rate G, and the power P have been normalized to $2\pi \times 16.7$ THz (the normalized Raman frequency is thus 0.78), 6.16 m^{-1}, and 616 W, respectively.

Another aspect of the Raman effect can be revealed by a computation of $|r_+(\omega)|^{-1}$ from Eq. (17), resulting in a value smaller than unity (Fig. 11). This means that in the presence of the Raman effect, the amplitude of the Stokes wave is larger than that of the anti-Stokes for the unstable mode, which is expected since the Raman gain tends to amplify the Stokes sideband while decreasing the anti-Stokes sideband.

IV. CONCLUSION

In conclusion, we studied MI by linearization around a nonlinear steady-state solution of the (nonlinear) Maxwell equation system. This steady-state solution corresponds to a cw pump. Specifically, the resulting linear partial differential equation is solved by harmonic analysis. In essence, the solution to this linear partial differential equation is a multiscale approximation according to the pump amplitude. Thus, unlike the traditional NSE-type methods, which involve Taylor expansions in frequency space, our result can be uniformly applied in any frequency range. Nonlinear dispersion and nonparametric effects such as Raman gain are formally included. We then applied the result to the case of various dispersion-flattened fibers to study the effects of the shape of the modal dispersion curve on MI. We found that when the fiber is flattened in the anomalous dispersion region, the instability is the superposition of a conventional MI and FWM at low pump power. These instability regions in frequency space merge at a large power. Instability also occurs even when the pump is in the normal dispersion, if the region is flattened. At low pump power it reduces to the conventional FWM instability. The frequency positions, the bandwidth, the maximum growth rate of the instability for various pump powers, etc., were characterized analytically. The Raman effect on these parametric instabilities was also studied. It changes the growth rate of the instability and makes the Stokes sideband stronger than the anti-Stokes sideband for the instability.

ACKNOWLEDGMENTS

G. P. A. was supported by the Army Research Office under the University Research Initiative Program. C. J. M. and M. Y. were supported by the National Science Foundation under Contract No. PHY-9057093, the U. S. Department of Energy (DOE) Office of Inertial Confinement Fusion under Cooperative Agreement No. DE-FC03-92SF19460, the University of Rochester, and the New York State Energy Research and Development Authority.

[1] H. C. Yuen and B. M. Lake, in *Advances in Applied Mechanics,* edited by C. S. Yih (Academic, New York, 1982), Vol. 22, p. 180.
[2] G. P. Agrawal, *Nonlinear Fiber Optics,* 2nd ed. (Academic, Boston, 1995).
[3] A. Hasegawa, in *Plasma Instabilities and Nonlinear Effects* (Spring-Verlag, Berlin, 1975).
[4] L. F. Mollenauer, R. H. Stolen, and J. P. Gordon, Phys. Rev. Lett. **45**, 1095 (1980).
[5] M. N. Islam, S. P. Dijaili, and J. P. Gordon, Opt. Lett. **13**, 518 (1988).
[6] E. J. Greer, D. M. Patrick, P. G. J. Wigley, and J. R. Taylor, Opt. Lett. **15**, 851 (1990).
[7] S. B. Cavalcanti, J. C. Cressoni, H. R. da Cruz, and A. S. Gouveia-Neto, Phys. Rev. A **43**, 6161 (1991).
[8] I. M. Uzunov, Opt. Quantum Electron. **22**, 529 (1990).
[9] E. A. Golovchenko and A. N. Pilipetskii, J. Opt. Soc. Am. B **11**, 92 (1994).
[10] M. Nakazawa, K. Suzuki, and H. A. Haus, Phys. Rev. A **38**, 5193 (1988).
[11] R. W. Boyd, *Nonlinear Optics* (Academic, Boston, 1992).
[12] V. A. Bhagavatula, M. S. Spotz, W. F. Love, and D. B. Keck, Electron. Lett. **19**, 317 (1983).
[13] A. H. Nayfeh, *Introduction to Perturbation Techniques* (Wiley, New York, 1981).
[14] M. Yu, C. J. McKinstrie, and G. P. Agrawal, Phys. Rev. E **48**, 2178 (1993).
[15] C. J. McKinstrie, X. D. Cao, and J. S. Li, J. Opt. Soc. Am. B **10**, 1856 (1993), and references therein.